Energy Conversion and Management: X 30 (2026) 101828

Contents lists available at ScienceDirect

Energy Conversion and Management: X

journal homepage: www.sciencedirect.com/journal/energy-conversion-and-management-x

Comparative performance evaluation of biomass chemical looping against conventional gasification technologies

Avishek Goel [a,*], Fabiola Panitz [b], Elyas M. Moghaddam [c], Jochen Ströhle [b], Bernd Epple [b], Chao He [a], Jukka Konttinen [a]

[a] Materials Science and Environmental Engineering, Faculty of Engineering and Natural Sciences, Tampere University, Tampere, Finland
[b] Technical University of Darmstadt, Department of Mechanical Engineering, Institute for Energy Systems and Technology, Germany
[c] Faculty of Mechanical Engineering, Process and Energy Department, Delft University of Technology, Netherlands

ARTICLE INFO

Keywords:
Chemical looping
Gasification
Syngas
Fluidized bed
Biomass

ABSTRACT

Biomass chemical looping gasification (BCLG) is emerging as a promising alternative to conventional gasification, addressing inherent limitations. This study systematically compares BCLG with conventional methods like air and air/steam gasification, using pine forest residue in an allothermal fluidized bed reactor. Key operational parameters such as reactor temperature (800–900 °C), equivalence ratio (0.18–0.36) and steam-to-biomass ratio (1.3) were examined. Performance indicators such as gas composition, yields, carbon conversion, and cold gas efficiency were evaluated and compared. BCLG without steam displayed similar performance to conventional methods. However, the performance of BCLG with steam surpassed conventional gasification methods and emerged as the most promising process. The results suggest enhanced catalytic performance of nickel smelter slag for reforming reactions under steam-rich conditions, with H_2/CO ratio, product gas yield, cold gas and carbon conversion efficiency improved by approximately 111%, 30%, 14% and 2%, respectively, compared to air/steam gasification.

1. Introduction

The urgent need to address climate change and global warming, exacerbated by excessive human energy consumption, has catalyzed scientific investigations towards developing sustainable alternatives to fossil fuels. Concurrently, a primary objective outlined in the Paris Agreement involved the production of advanced biofuels derived from renewable sources, serving as substitutes for fossil fuels and facilitating the reduction of green house gas emissions [1]. Among the array of potential alternatives, syngas production via biomass gasification emerges as a promising solution, with its demand witnessing an upward trend [2]. Additionally, syngas holds considerable promise for various applications, including power generation and heating, while also offering the potential for conversion into high-value products such as Fischer-Tropsch liquids, synthetic natural gas, hydrogen, and other various chemicals [3,4].

Biomass can be converted into syngas through conventional gasification methods involving the use of air, pure oxygen and/or steam as gasification media. However, these methods suffer from significant drawbacks such as (i) generation of N_2-diluted low-quality product gas when using air as the gasification medium [5], (ii) increased costs due to the requirement of energy-intensive and expensive air separation units (ASUs) to provide pure oxygen for yielding high-quality product gas [6] and (iii) limited efficiency and high heat requirements when using steam as the gasification medium [6–8]. Circumventing these challenges, Biomass Chemical Looping Gasification (BCLG) emerges as a promising solution, offering economic viability, high efficiency and low emissions [5]. By employing an oxygen carrier (OC) instead of air, BCLG generates N_2-free high-quality syngas [9,10], which reduces the need for expensive ASUs [11–13]. Moreover, BCLG benefits from the catalytic properties of reduction products from OCs, which promote tar cracking and lower tar content in the product gas [14,15]. Additionally, certain OCs facilitate the conversion of NH_3 and NO_x precursors into harmless N_2, which reduces emissions [15,16]. BCLG also possesses inherent CO_2 separation and capture capabilities, which makes it a low-emission technology for syngas production [5].

In general, chemical looping involves splitting a chemical reaction into multiple successive reactions which occur in separate reactors with the exchange of a recyclable intermediate material. In the context of

* Corresponding author.
E-mail address: avishek.goel@tuni.fi (A. Goel).

https://doi.org/10.1016/j.ecmx.2026.101828
Received 26 July 2025; Received in revised form 27 February 2026; Accepted 7 April 2026
Available online 7 April 2026

Nomenclature

a.r.	As Received
ASU	Air Separation Unit
BCLG	Biomass Chemical Looping Gasification
BCLGO	Biomass Chemical Looping Gasification without steam
BCLGS	Biomass Chemical Looping Gasification with steam
CBGA	Conventional Biomass Gasification using air
CBGAS	Conventional Biomass Gasification using air and steam
CCE	Carbon Conversion Efficiency
CGE	Cold Gas Efficiency
d.b.	Dry Basis
ER	Equivalence ratio
LHV	Lower Heating Value
NS1100	Nickel Smelter Slag calcinated at 1100 °C
OC	Oxygen Carrier
OCBR	Oxygen Carrier to Biomass Ratio
PFR	Pine Forest Residue
PGY	Product Gas Yield
SBR	Steam to Biomass Ratio
SGY	Syngas Yield

BCLG, this concept is applied to indirectly supply oxygen from the atmosphere to the biomass feedstock, which contrasts conventional gasification method (see Fig. 1). As an example, the conventional biomass gasification reaction (E1) is typically carried out in a single reactor. However, in BCLG, this reaction is divided into two sub-reactions (E2 and E3) occurring in distinct fuel and air reactors. The OC material, such as OC1, undergoes reduction to OC2 by reacting with the biomass volatiles in the fuel reactor (E1) and is subsequently reoxidized by combusting with air in the air reactor (E2). The reoxidized carrier (OC1) circulates back to the fuel reactor, carrying oxygen and heat, thereby forming a closed loop between the interconnected reactors.

BCLG has emerged as a promising technology for syngas production, with researchers exploring a wide range of feedstocks and OC types across various reactor methods [10,17–28]. More recently, BCLG has made considerable progress toward scale-up with pilot-scale demonstration. In early 2026, BCLG tests were successfully conducted at a 5 MW_{th} scale, where the reactor demonstrated stable autothermal operation for over 40 h using ilmenite as the oxygen carrier [29]. Complementing this milestone, several pilot test campaigns at approximately 1 MW_{th} scale have also been carried out, showcasing BCLG with more than 400 h of cumulative autothermal operation using biogenic residues [30].

Investigations have encompassed diverse feedstocks including woody biomass, terrestrial waste, residential waste and agricultural waste, while employing OC materials ranging from natural ores to synthetic substances and waste materials. These investigations were implemented across multiple reactor systems such as fixed bed, bubbling fluidized bed and dual fluidized bed configurations (refer to Table 1). Notably, further details about the mentioned studies can be found at Goel et al. [5]. Throughout these investigations, the advantages of BCLG such as enhanced catalytic activity, heightened char gasification, improved gasification efficiency and generation of higher quality product gas over conventional gasification methods have been extensively discussed. However, a comparative experimental study which directly benchmarks BCLG against conventional gasification methods is notably absent in the literature. The primary objective of the present study is to conduct a comprehensive comparative examination of BCLG performance in contrast to conventional gasification methods, aiming to conclusively validate its advantages. Notably, the results used in benchmarking were experimentally obtained using the same fluidized bed reactor and under comparable gasification conditions.

Table 1
Overview of selected BCLG studies.

Reactor type	Process conditions	Feedstock	OC material(s)	Ref.
Interconnected dual FB reactors	Temperature: 650–1000 °C OC/feed: ≈ 4–20 OC/bed material: ≈ 0.2–0.6	Pinewood, Pine sawdust, Rice husk, Rice straw	Iron-olivine, Fe_2O_3/Al_2O_3, Fe_2O_3. NiO/Al_2O_3, NiO/Al_2O_3, CaO.NiO/Al_2O_3	[2,18,21,30]
Coupled BFB and CFB reactor, Fixed bed, Fluidized bed, TGA, Furnace	Temperature: 30–1200 °C OC/feed: ≈ 0.2–11.5	Biomass sawdust, Polyethylene, Pine char, Pine sawdust and wood, Sewage Sludge, Wheat straw, Rice straw, Rice husk, Microalgal residue, Water hyacinth, Kitchen waste, Swine manure	CaO, NiO, Fe_2O_3, Fe_2O_3. support (Al_2O_3, SiO_2, TiO_2, ZrO_2), Hematite, NiO.Fe_2O_3, Red mud, Fe_2O_3/CuO, Fe_2O_3/CaO, Sludge ash, Copper slag, Copper ore	[2,7,31–43]

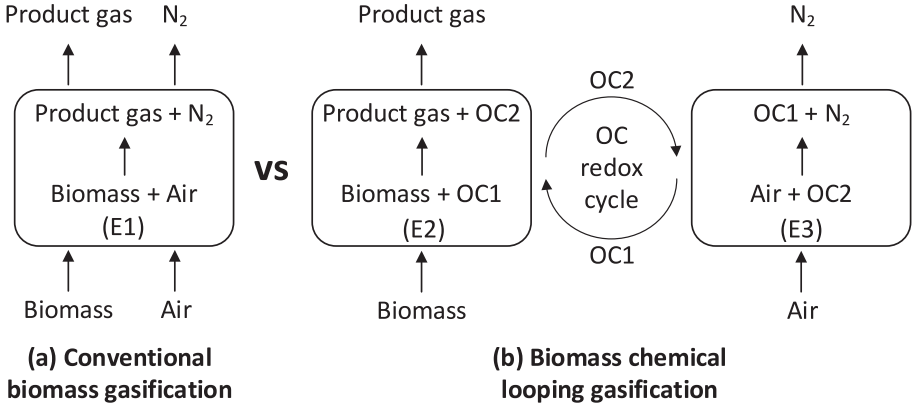

Fig. 1. Schematic illustration comparing the reactions in conventional biomass gasification and biomass chemical looping gasification technologies.

Building upon the findings of our previous study on evaluating the performance of BCLG using industrial waste as OC [43], which explored the utilization of nickel smelter slag as an OC and investigated the influence of critical operating parameters (e.g., reactor temperatures, oxygen carrier-to-biomass ratio (OCBR) and addition of steam as a gasification medium). In a previous study, BCLG experiments using pine forest residue (PFR) were conducted in a fluidized bed reactor, with nickel smelter slag calcined at 1100 °C serving as the OC to evaluate and optimize the process. The optimal gasification conditions were identified as a reactor temperature of 850 °C, an OC-to-biomass ratio of 10:1, and a steam-to-biomass ratio of 1.4. Under these conditions, high-quality product gas was obtained, with concentrations of 38.9 vol% H_2, 19.7 vol% CO, 34.5 vol% CO_2, and 6.6 vol% CH_4.

This study extends the analysis to include conventional gasification methods utilizing air and air/steam as the gasification medium. The investigations were conducted in a fluidized bed reactor using PFR as feedstock. In this study, the impact of similar critical operating parameters on conventional gasification methods is examined. Gasification performance is evaluated in terms of product gas compositions, product and syngas yields, carbon conversion and cold gasification efficiencies. More importantly, a comprehensive assessment is conducted, comparing gas compositions, gas yields and system efficiencies across all gasification methods, including both BCLG (from previous study) and conventional techniques, and determine the most suitable method.

It is important to note that the selection of nickel smelter slag was based on a detailed investigation and comparison of the physical and chemical properties of several low-cost materials, including copper slag, steel converter slag, ladle slag, desulphurization slag, manganese ore and sewage sludge ash [44]. The materials were evaluated based on their characterization, reactivity, selectivity, mechanical strength and sintering behavior. Nickel smelter slag is generated as a by-product during the nickel smelting process, either through water quenching or natural cooling of molten material during nickel extraction. Approximately 6–16 tons of slag are produced per ton of nickel, resulting in a global annual production of roughly 16–40 million tons [45]. Despite this large output, its utilization rate remains low, at around 10 wt% [44]. The nickel smelter slag used in this study was calcined at 1100 °C.

2. Materials and methods

2.1. Materials and characterization

In this investigation, PFR was utilized as the biomass feedstock. PFR pellets (received from Techincal University of Darmstadt, Germany) was ground and seived upto a particle size of 2000 μm (particle size distribution shown in Fig. A1 in the supplementary document). The characteristics of PFR are outlined in Table 2. The PFR is composed of bark and pine needles and was sourced from Sweden. Concurrently, silica sand was chosen as the inert bed material for fluidization during the gasification process. The silica sand particles exhibited a particle diameter of ≤355 μm and a bulk density of 2602.8 ± 16.7 kg/m^3. Additionally, minimum fluidization velocity was determined to be 0.04 m/s.

Table 2
Characteristics of pine forest residue.

Particular	Unit	Value
Proximate and ultimate analysis		
Moisture content	(wt%, a.r.)	4.4
Fixed carbon	(wt%, a.r.)	16.6
Volatiles	(wt%, a.r.)	76.8
Ash	(wt%, a.r.)	2.2
C	(wt%, d.b.)	52.3
H	(wt%, d.b.)	6.2
O	(wt%, d.b.)	40.9
S	(wt%, d.b.)	0.03
N	(wt%, d.b.)	0.5
Cl	(wt%, d.b.)	0.01
Lower Heating Value, LHV	(MJ/kg, d.b.)	19.1
Minimum fluidization velocity, u_{mf}	(m/s)	0.05

2.2. Experimental setup and procedure

The experimental investigation was conducted in a ~0.5 kW_{th} fluidized bed reactor setup located at the Technical University of Darmstadt in Germany. The schematic diagram depicting the reactor setup is presented in Fig. 2. The primary reactor body comprises a cylindrical column with an internal diameter of 54.5 mm and a height of 1000 mm. To ensure precise control and monitoring, temperature and pressure sensors were strategically positioned along the length of the reactor. Additionally, external heating elements were employed to heat the reactor. A gas distribution unit regulated the flow and mixing of inlet gases (e.g., N_2 and air for the case of conventional gasification, and N_2 for the case of chemical looping gasification). The inlet gases, along with steam, were mixed in the pre-heating zone before entering the gasification zone through a porous gas distribution plate for fluidizing the bed. Biomass feedstock was continuously fed into the gasification zone at a specified height above the gas distribution plate using a dual screw-feeding system. The resulting gases were directed through an externally heated post-heating zone before entering a gas filtering and washing unit to remove impurities and tars. Finally, the gases were directed to the exhaust line, with a portion diverted for real-time volumetric gas composition analysis using ABB URAS 206 and ABB Caldos 27 analyzers. The concentrations of CO, CO_2, and CH_4 were continuously measured using a non-dispersive infrared sensor integrated into the ABB URAS 26 unit. Additionally, H_2 concentration was determined using a ABB Caldos 27 thermal conductivity analyzer. Notably, a comprehensive description of the fluidized bed reactor setup, including a detailed schematic diagram, is available in our previous study [43].

An experimental procedure similar to that described in our previous study was followed [43]. In the previous work, oxygen was supplied using an OC material; nickel smelter slag calcined at 1100 °C (NS1100). In the present study, however, air was used as the oxygen source. When oxygen was supplied using the OC, the PFR and NS1100 were blended in a predetermined ratio prior to the experiment, and the resulting mixture

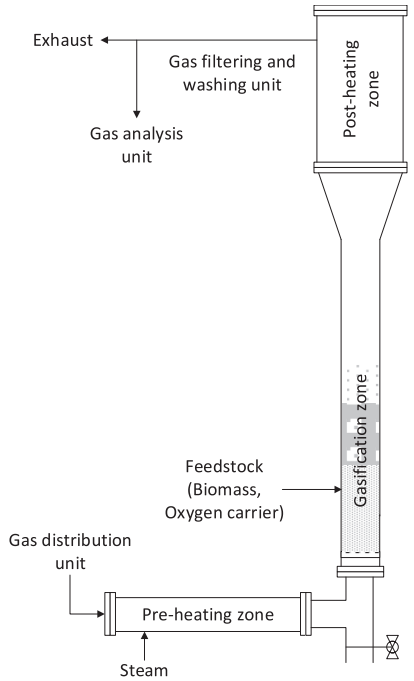

Fig. 2. Schematic diagram of the 5kW_{th} fluidized bed reactor setup at the Technical University of Darmstadt.

was loaded into the feed hopper. This ratio corresponded to a specific equivalence ratio (ER), calculated based on the oxygen transport capacity of NS1100 (~3.3%). The oxygen transport capacity of NS1100 was experimentally determined using the H_2 temperature program reduction method at temperatures between 800 °C and 900 °C. For experiments utilizing air, the required amount of air was mixed with an N_2 stream (purity of 99.9%) and introduced into the reactor through a porous gas distribution plate, as dictated by the experimental design.

In the study, the gasification of PFR was examined, which focused on three crucial operational parameters: reactor temperature, steam-to-biomass ratio (SBR) and equivalence ratio. During the experiment, ER was systematically varied between 0.18 and 0.36 under three different reactor temperatures (800, 850 and 900 °C). Furthermore, the effect of steam addition was investigated for an SBR of 1.3. Throughout the experiments, the biomass feedrate remained constant with a value of 1.1 g/min. A summary of the operational parameters is presented in Table 3. Notably, u_f and u_{mf} denote the superficial velocity (m/s) and the minimum fluidization velocity (m/s), respectively. The average composition values were considered after the reactor reached steady-state conditions and the gas compositions stabilized. The average values were calculated over a period of 600 s, with measurements recorded every 5 s.

2.3. Data evaluation

Various performance indicators were utilized to compare and evaluate the performance of different gasification methods. These indicators include product gas composition, H_2/CO ratio, product gas and syngas yields, carbon conversion and cold gas efficiencies. The calculation method for the mentioned indicators are discussed below. Note that the carbon mass balance calculations could not be performed for the experiments, as the bed material (consisting of a unquantifiable mix of hydrocarbons, reduced OC, and silica sand) got accumulated during the entire experimental run and could only be collected at the end of each run.

The composition of product gas (CO, H_2, CO_2, and CH_4) was determined by deducting the volume fraction of N_2 from the overall gas composition. It was assumed that the introduced N_2 is inert and remains unconsumed throughout the process. The dry and N_2-free product gas composition (Ci, vol%) was calculated using the following equation:

$$C_{i_{N2-free}} = \frac{C_i}{100 - \sum_{all} C_i} \tag{1}$$

where, the dry volume fraction of component i (vol%) is denoted by C_i. Furthermore, the H_2/CO ratio was calculated using the outlet gas composition for H_2 and CO according to the following equation:

$$\frac{H_2}{CO} = \frac{C_{H_2}}{C_{CO}} \tag{2}$$

The volumetric flowrate of product gases ($V_{i,out}$, Nm^3/h) was calculated by balancing N_2 concentrations between inlet and outlet gases (N_2, considered as an inert tracer gas), using the following equation:

$$V_{i,\ out} = C_i \times \frac{V_{N_2,\ in}}{C_{N_2}} \tag{3}$$

where, inlet volume flowrate of N_2 (Nm^3/h) is denoted by $V_{N2,in}$ and dry volume fraction of of N_2 (vol%) recorded by gas analysis unit is represented by C_{N2}. Moreover, the yields of product gas (Y_{pg}, Nm^3/kg-bio) and syngas (Y_{sg}, Nm^3/kg-bio) were determined using the following equations:

$$Y_{pg} = \frac{V_{H_2,\ out} + V_{CO,out} + V_{CO_2,\ out} + V_{CH_4,\ out}}{m_b} \tag{4}$$

$$Y_{sg} = \frac{V_{H_2,\ out} + V_{CO,out}}{m_b} \tag{5}$$

where, volumetric flowrate of individual gas components is denoted by $V_{i,out}$ (Nm^3/h), respectively. Furthermore, carbon conversion efficiency (CCE, %) is defined as the proportion of carbon converted (CO, CO_2 and CH_4) from the carbon in biomass fed into the reactor and it was calculated through the following equation:

$$CCE = \frac{\left(N_{CO,out} + N_{CO_2,\ out} + N_{CH_4,\ out}\right) \times 12}{m_b \times C_{\%}} \times 100 \tag{6}$$

where, the molar flowrate of individual gas component i is denoted by N_i (kmol/h) denotes, the biomass feedrate to the reactor is represented by m_b (kg/h) and the carbon content present in biomass is represented by ($C_{\%}$, wt%). Additionally, cold gas efficiency (CGE, %) is defined the ratio of chemical energy within the product gas to the total energy of the biomass and it was computed as follows:

$$CGE = \frac{LHV_{pg} \times Y_{pg}}{LHV_b} \times 100 \tag{7}$$

where, denotes lower heating value (LHV, MJ/Nm^3) and yield of product gas is denoted by LHV_{pg} and Y_{pg}, respectively. LHV (MJ/kg) of biomass is represented by LHV_b.

3. Results and discussion

3.1. Pressure and temperature distribution

The gasification of PFR using air and/or steam was investigated utilizing the fluidized bed reactor setup. The reactor pressures (P1, P2 and P3) and temperatures (T1, T2 and T3) at different reactor heights (130 mm, 350 mm and 550 mm) were continuously monitored throughout the reaction period (see Fig. A2 in supplementary document). Generally, the average recorded temperature during the experimental run was 805.3 ± 10 °C, 855.4 ± 15.6 °C, and 896.9 ± 10.4 °C when the reactor temperature was set to 800 °C, 850 °C and 900 °C. Generally, pressures P1, P2 and P3 exhibited fluctuations within the ranges of 95.9–128.9 mbar, 64.4–114.9 mbar, and 20.1–44.5 mbar, respectively. The consistency in reactor temperature and pressure fluctuations collectively indicates that the reactor operated stably throughout the experimentation period, ensuring reliable data acquisition.

Table 3
Experimental matrix for conventional biomass gasification.

Parameter	Unit	Value								
Reactor temperature	(°C)	800	850	850	850	850	900	800	850	900
Biomass feedrate	(g/min)	1.1	1.1	1.1	1.1	1.1	1.1	1.1	1.1	1.1
N_2 flowrate	(Nm^3/h)	0.22	0.22	0.25	0.21	0.19	0.22	0.19	0.19	0.19
Equivalence ratio	(−)	0.27	0.27	0.18	0.3	0.36	0.27	0.27	0.27	0.27
SBR	(−)	–	–	–	–	–	–	1.4	1.4	1.4
u_f/u_{mf}	(−)	3.6	3.8	3.8	3.8	3.8	4.0	4.6	4.8	5.0
Silica sand	(g)	2000	2000	2000	2000	2000	2000	2000	2000	2000

3.2. Effect of operational parameters on the performance of biomass gasification

3.2.1. Reactor temperature

Reactor temperature acts as a critical parameter in biomass gasification. It significantly influences the reaction kinetics and subsequently affects key performance indicators such as gas composition, gas yield, carbon conversion and cold gasification efficiencies. In the experimental study, the influence of reactor temperature was examined across three different temperatures (i.e., 800, 850 and 900 °C). The investigation was conducted under a constant ER of 0.27 and biomass feedrate of 1.1 g/min.

Fig. 3 illustrates the volumetric composition of dry and N_2-free product gas across varying reactor temperatures. As the temperature increased, an evident change in the product gas composition was observed: H_2 concentration significantly increased from 17.9 to 25.8 vol %, CO concentration moderately increased from 37.2 to 39.9 vol%, CO_2 concentration notably decreased from 37.4 to 27.9 vol% and CH_4 concentration slightly decreased from 7.5 to 6.5 vol%. The trends were similar to the findings reported by Liu et al. [46]. The observed variations can be attributed to a complex and competing interplay of endothermic and exothermic reactions, as represented by equations R(1)–R(8). These equations are governed by Le Chatelier's principle, wherein high temperatures drive the equilibrium towards the product and the reactant side in endothermic and exothermic reactions, respectively.

The endothermic reactions, such as the pyrolysis reaction (R1), the Boudouard reaction (R2), the water–gas reaction (R3) and steam-methane reforming reactions (R5), partly contribute to the increase in H_2 and CO concentrations at higher temperatures. Additionally, the rise in CO concentration can be attributed to the exothermic water–gas shift reaction (R4). Conversely, the decrease in CO_2 concentration can be explained by the endothermic Boudouard reaction (R2) and the exothermic water–gas shift reaction (R4), which counterbalance the CO_2 production effect of the pyrolysis reaction (R1). The slight decrease in CH_4 concentration can be attributed to the steam-methane reforming reaction (R5), which counteracts the effect of CH_4 production during pyrolysis (R1). Moreover, the significant increase in H_2 production with increased temperature supports the occurrence of the steam-methane reforming reaction (R5).

$$\text{Biomass} \rightarrow \text{Gas}\left(CO, H_2, CO_2, CH_4, C_xH_y\right) + \text{Char} + \text{Ash} + \text{Tar} + H_2O \quad \text{(R1)}$$

$$C + CO_2 \leftrightarrow 2CO (\Delta H = +172\,\text{MJ/kmol}) \quad \text{(R2)}$$

$$C + H_2O \leftrightarrow CO + H_2 (\Delta H = +131\,\text{MJ/kmol}) \quad \text{(R3)}$$

$$CO + H_2O \leftrightarrow CO_2 + H_2 (\Delta H = -41\,\text{MJ/kmol}) \quad \text{(R4)}$$

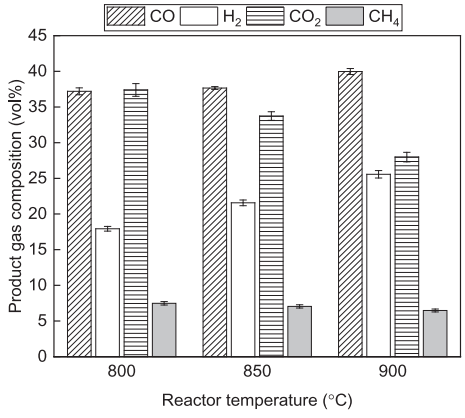

Fig. 3. Effect of reactor temperature on product gas composition at equivalence ratio of 0.27.

$$CH_4 + H_2O \leftrightarrow CO + 3H_2 (\Delta H = +206\,\text{MJ/kmol}) \quad \text{(R5)}$$

$$C + 0.5O_2 \rightarrow CO (\Delta H = +172\,\text{MJ/kmol}) \quad \text{(R6)}$$

$$CO + 0.5O_2 \rightarrow CO_2 (\Delta H = -284\,\text{MJ/kmol}) \quad \text{(R7)}$$

$$H_2 + 0.5O_2 \rightarrow H_2O (\Delta H = -242\,\text{MJ/kmol}) \quad \text{(R8)}$$

Fig. 4 displays the variations in product gas yield, syngas yield, CCE and CGE for the studied reactor temperature range. It is evident that the values of all the mentioned gasification performance parameters increased with the increase in reactor temperature. This phenomenon can be ascribed to the intensified endothermic pyrolysis (R1), Boudouard (R2) and water–gas reaction (R3) at elevated temperatures. These reactions promote the conversion of carbon into product gas, which consequently leads to increased product gas yield and CCE [46]. Furthermore, the elevated concentrations of combustible gases with increased temperature, as discussed above, contributed to the increase in syngas yield and CGE. Additionally, high temperatures may have promoted additional biomass tar cracking [18,46], which aided in the improved gasification performance. Overall, a reactor temperature of 900 °C emerged as optimal, characterized by the highest values of key gasification performance indicators.

3.2.2. Equivalence ratio

The ER refers to the fraction of actual oxygen to biomass compared to the stoichiometric oxygen required for complete oxidation and serves as a crucial parameter in assessing gasification performance. Its effect was examined by varying ER within the range of 0.18 to 0.36 at a constant reactor temperature of 850 °C and biomass feedrate of 1.1 g/min.

Fig. 5 shows the variation in product gas composition across varying ER values. Across the range of ER studied, the concentrations of CO and H_2 exhibited an overall decrease. However, at an ER of 0.3, both CO and H_2 concentrations slightly increased before decreasing again. Conversely, the concentration of CO_2 increased overall across the studied range, with a slight decrease observed at an ER of 0.3, followed by an increase. Regarding CH_4, its concentration consistently decreased with increasing ER values. Similar trends were reported in previous research studies by Niu et al. [47] and Han et al. [48]. This trend can be explained by the complex interplay of two opposite effects represented by reactions (R(7), R8 and R1-R3, R5). On one hand, higher ER values enhanced the availability of oxygen for reactions with volatiles, which led to intensified oxidation reactions (R(7), R8) and the consumption of

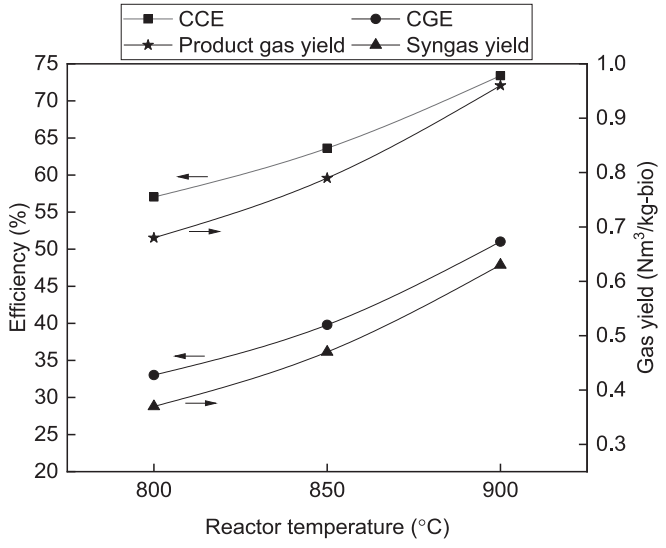

Fig. 4. Effect of reactor temperature on product gas and syngas yields, carbon conversion and cold gasification efficiency at equivalence ratio of 0.27.

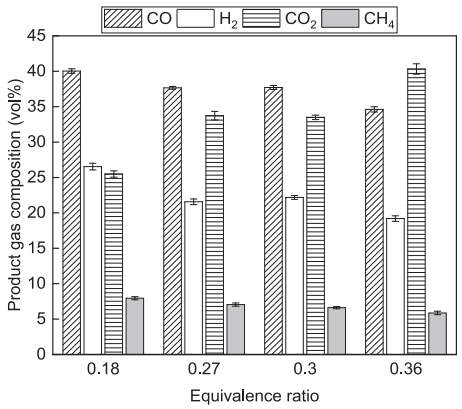

Fig. 5. Effect of equivalence ratio on product gas composition at reactor temperature of 850 °C.

combustible gases. On the other hand, the strengthened oxidation reactions released more energy, which was utilized to support pyrolysis (R1), Boudouard (R2), water–gas (R3) and steam-methane reforming (R5) reactions. Consequently, this resulted in the generation of more CO and H_2 and the consumption of CH_4.

Additionally, the variation of product gas yield, syngas yield, CCE and CGE for different ER values is depicted in Fig. 6. It was observed that product gas yield and CCE increased with higher ER values due to enhanced carbon conversion (see reactions R1-R3 and R5). Furthermore, syngas yield and CGE increased to maximum values at 0.3, followed by a decrease. This behavior is collectively attributed to the variation in the concentration of combustible gases (i.e., CO, H_2 and CH_4), as discussed previously. In summary, it can be concluded that an ER of 0.3 represents an optimal value, as it facilitated a balanced product gas composition with saturated value of CCE and the highest syngas yield, product gas yield and CGE values.

3.2.3. Steam addition as a gasification medium

In the study, the impact of steam addition on biomass gasification performance was systematically examined. Steam, which serves as an additional oxygen source, holds potential for enhancing the gasification process [49]. To investigate this, a constant steam flow rate of 1.5 g/min and a PFR feed rate of 1.1 g/min were maintained while examining the influence of steam addition at reactor temperatures of 800, 850 and 900 °C.

The impact of steam addition on the product gas composition across the three reactor temperatures is depicted in Fig. 7. Irrespective of the reactor temperature, a substantial increase in H_2 concentration was observed, while CO_2 and CH_4 concentrations displayed moderate increments and CO concentration decreased significantly upon steam addition. Similar trends in product gas composition were reported by Hernández et al. [50] and Nguyen et al. [51]. These variations can be ascribed to a sequence of gasification reactions influenced by increased steam concentration in the reactor. Steam addition accelerated the water–gas (R3) and steam-methane reforming (R5) reactions, which led to increased production of H_2 and CO. However, the generated CO was consumed by the accelerated water–gas shift reaction (R4), which resulted in increased CO_2 production and a decreased CO fraction. Moreover, the increase in CH_4 concentration with steam addition may be attributed to the higher H_2 levels, which could have promoted the methanation reaction (R9) and the hydrogasification reaction (R10), resulting in additional CH_4 formation [50]. Upon analyzing the trend of product composition for varying reactor temperatures, it was observed that the concentration of H_2 significantly increased, whereas that of CO_2 decreased, and the concentrations of CH_4 and CO remained relatively unchanged. This observation could be attributed to the intensification of endothermic reactions (R(2), R3 and R5) with an increase in temperature, which resulted in elevated H_2 and CO concentrations and a reduced CO_2 concentration. However, the introduction of steam facilitated the water–gas shift reaction (R4), which lead to the consumption of the produced CO.

$$2CO + 2H_2 \leftrightarrow CH_4 + CO_2\,(\Delta H = -247\,MJ/kmol) \quad (R9)$$

$$C + 2H_2 \leftrightarrow CH_4\,(\Delta H = -74.8\,MJ/kmol) \quad 10)$$

The effect of steam addition was further examined by analyzing key gasification performance indicators, including product gas yield, syngas yield, CCE and CGE, as listed in Table 4. Across all three reactor temperatures, these performance indicators significantly increased when steam was introduced into the reactor. The improved CCE and product gas yield could mainly be attributed to the acceleration of the water–gas reaction, which directly impacted the conversion of carbon. Additionally, the increase in syngas yield and CGE can be explained by the considerable increase in H_2 concentration and moderate rise in CH_4 concentration. This increase compensated for the loss of CO and consequently improved gas yield and chemical energy. In conclusion, the addition of steam as a gasification medium significantly enhanced the gasification performance. Among the results investigated under steam-rich conditions, a reactor temperature of 900 °C emerged as an optimal value. This conclusion is supported by the highest H_2

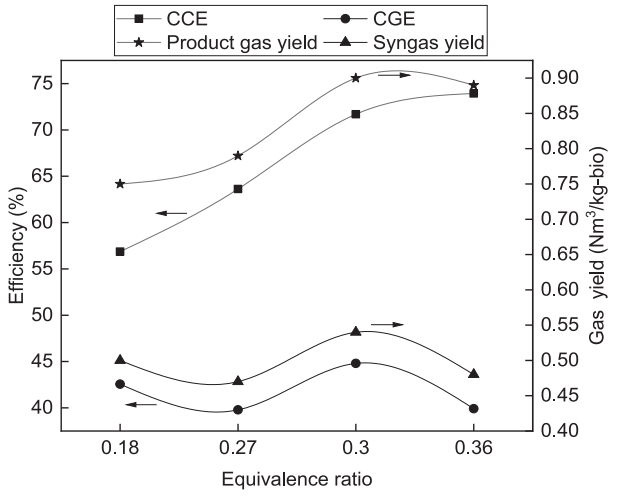

Fig. 6. Effect of equivalence ratio on product gas and syngas yields, carbon conversion and cold gasification efficiency at reactor temperature of 850 °C.

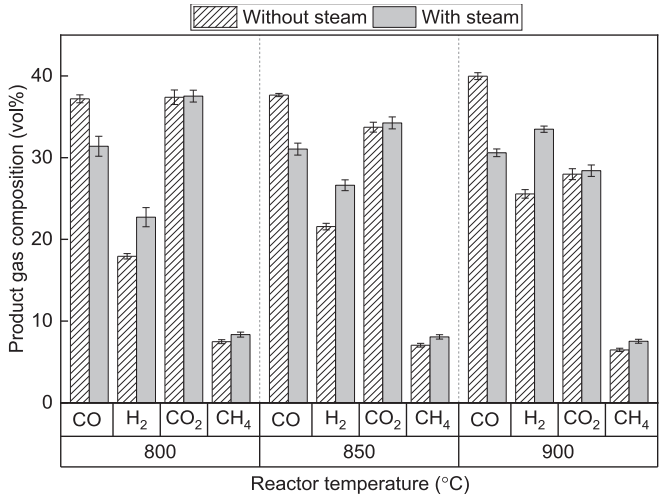

Fig. 7. Effect of steam addition on product gas composition at reactor temperatures of 800 °C, 850 °C and 900 °C.

Table 4
Effect of steam addition on product gas yield, syngas yield, carbon conversion and cold gasification efficiency at reactor temperatures of 800 °C, 850 °C and 900 °C.

Parameter	Unit	Reactor temperature (°C)					
		800		850		900	
Gasification agent	(−)	Without steam	With steam	Without steam	With steam	Without steam	With steam
Product gas yield	(Nm^3/kg-bio)	0.68	1.01	0.79	1.01	0.96	1.21
Syngas yield	(Nm^3/kg-bio)	0.37	0.56	0.47	0.58	0.63	0.77
CCE	(%)	57.04	79.64	63.62	76.44	73.40	82.49
CGE	(%)	33.03	49.94	39.79	51.51	51.02	64.40

concentration, product gas yield, syngas yield, CCE and CGE.

3.3. Comparative analysis of chemical looping and conventional gasification methods

Chemical looping gasification (CLG) has gained interest for its suggested superior performance compared to conventional gasification methods as it promises the production of high-quality product gas and enhanced gasification efficiency. Nevertheless, it remains crucial to directly compare the performance metrics of the methods and validate the efficacy of CLG as a viable alternative. In this section, CLG has been rigorously compared against conventional gasification methods to gauge the potential benefits of CLG and identify areas that necessitate further improvement. The investigation was comprehensively conducted to compare critical performance parameters including product gas composition, H_2/CO ratio, product gas and syngas yields, as well as CCE and CGE.

3.3.1. Conventional biomass gasification using air vs biomass chemical looping gasification without steam

A comparison between conventional biomass gasification using air (CBGA) and biomass chemical looping gasification without steam (BCLGO) was conducted to compare the gasification behavior when oxygen was supplied using air and OC material, respectively. It is important to note that the BCLGO method was evaluated in this study primarily to isolate and examine the effect of oxygen supplied by NS1100, in contrast to oxygen provided by air. The results of this comparative study are illustrated in Fig. 8. The experiments for both methods were conducted under similar reactor conditions, with reactor temperatures of 800, 850 and 900 °C and a PFR feed rate of 1.1 g/min. To ensure a fair comparison, both gasification methods were operated at similar ER (~0.25–0.27). To achieve this, the CBGA process used an air flow rate of 0.09 Nm^3/h, while the BCLGO process maintained an OCBR of 10:1. An OCBR of 10:1 was concluded optimal in our previous study [43] which evaluated utlization of nickel smelter slag in BCLG.

Fig. 8(a) depicts the variation in product gas composition across reactor temperatures ranging from 800 to 900 °C. Notably, a consistent trend emerged across all temperatures, with CH_4 concentration remained higher under BCLGO compared to CBGA. The gap could be attributed to difference in the rates of partial and complete oxidation reactions of CH_4 (R11 and R12) between the two gasification methods. Specifically, the oxidation rate in BCLGO is observed to be lower than that in CBGA, which can be ascribed to the limited reaction time and reduced gas/solid interaction efficiency of the OC with CH_4 compared to air. This observation is corroborated by CFD investigations conducted by Deng et al. [52] and Sheth et al. [53], which highlighted the reduced concentration of OC in the freeboard region of the reactor in the chemical looping process. However, the ineraction of OC with volatiles could potentially be improved by optimizing the particle size and fluidization velocities, while preferably using circulating fluidized bed systems. Furthermore, due to the limited interaction between OC and CH_4 in BCLGO, a smaller proportion of CH_4 undergoes oxidation to form CO, CO_2 and H_2. It is evidenced by the higher concentration of CO and

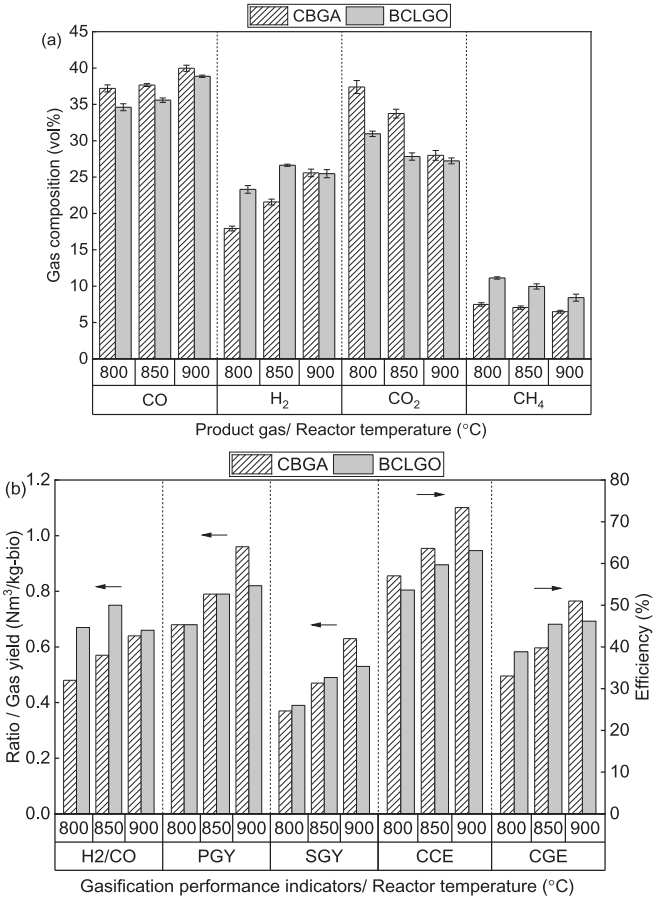

Fig. 8. Comparison of (a) product gas composition and (b) H_2/CO ratio, PGY, SGY, carbon conversion and cold gasification efficiency between conventional biomass gasification using air and biomass chemical looping gasification without steam. Here, PGY and SGY denotes product gas yield and syngas yields, respectively.

CO_2 observed in CBGA. However, the H_2 concentration in CBGA is lower than in BCLGO and can be ascribed to the oxidation of generated H_2 (R8) in the freeboard region. Interestingly, when the reactor temperature reached 900 °C, the difference in H_2 concentration between CBGA and BCLGO became minimal (≈ 0.1 vol%). It could be attributed to the increased reactor temperature, where higher temperature drove the equilibrium towards H_2O in the exothermic oxidation reaction (R8).

$$CH_4 + 0.5O_2 \leftrightarrow CO + 2H_2 \,(\Delta H = -36\,MJ/kmol) \quad 11)$$

$$CH_4 + 2O_2 \leftrightarrow CO_2 + H_2O \,(\Delta H = -803\,MJ/kmol) \quad 12)$$

Fig. 8(b) illustrates the variation in product gas and syngas yields, H_2/CO ratio, CCE and CGE for the studied temperature range. Across the temperatures investigated, it is evident that the product gas yield and

CCE were similar or lower in the case of BCLGO compared to CBGA. This observation suggests that more residual carbon was converted into product gas under CBGA, contradicting previous findings that suggested the presence of the OC promotes char conversion [5,7]. Additionally, the syngas yield was marginally higher for BCLGO compared to CBGA (≈ +0.02 Nm^3/kg-bio), except at 900 °C, where the syngas yield was lower for BCLGO than CBGA (≈ −0.1 Nm^3/kg-bio). The H_2/CO ratio and CGE under BCLGO were considerably higher than CBGA until 850 °C (H_2/CO ratio ≈ +0.19 and CGE ≈ +5.7%). However, H_2/CO became marginally higher (≈ +0.02) and CGE became lower (≈ −4.85%) than CBGA at 900 °C. These trends can be collectively understood by the variations in product gas concentrations of combustible gases (CO, H_2 and CH_4) and was discussed earlier in detail. Overall, it can be concluded that BCLGO did not exhibit any significant improvement in gasification performance compared to CBGA. However, until reactor temperature of 850 °C, the gasification performance of BCLGO was similar to CBGA. Nonetheless, further optimization and improvement of BCLGO performance could be achieved by investigating the influence of parameters (e.g., OC particle size and gas flowrates) which may affect the concentration of OC in the freeboard and consequently impact reactivity rates and reaction times.

3.3.2. *Conventional biomass gasification using air and steam vs biomass chemical looping gasification using steam*

Conventional biomass gasification using air and steam (CBGAS) and biomass chemical loooping gasification using steam (BCLGS) were thoroughly compared under similar experimental conditions to ensure uniformity. For both gasification methods, the experiments were conducted at reactor temperatures ranging from 800 to 900 °C, with a constant PFR feed rate of 1.1 g/min and an SBR of 1.3 to 1.4. For CBGAS, the air flow rate was maintained at 0.09 Nm^3/h, while for BCLG, the OCBR was consistently maintained at 10:1. The comparison results are presented in Fig. 9.

Analysis of Fig. 9(a) revealed distinct trends in product gas composition between BCLGS and CBGAS. Notably, under BCLGS, a significant increase in H_2 concentration and decrease in CO concentration compared to CBGAS is observed, which indicated a catalytic effect of the OC in promoting the water–gas shift reaction (R4) [54]. Additionally, at reactor temperatures of 850 and 900 °C, BCLGS demonstrated lower CH_4 concentrations compared to CBGAS (≈ −1.5 and ≈ −0.5 vol%, respectively), which suggested catalysis of the steam-methane reforming reaction (R5) by the OC. However, as the reactor temperature reached 900 °C, the reforming effect weakened, possibly due to partial deactivation of the OC through thermal sintering. This observation aligns with findings discussed in the study by Goel et al. [43], which highlighted the increased effect of higher temperatures and steam addition on the acceleration of thermal sintering and agglomeration tendencies in the OC. To investigate the behavior of sintering and agglomeration, the specific surface area and total pore volume of the OC were examined. It was observed that both properties decreased (e.g., specific surface area, 1.412 →0.261 m^2/g and total pore volume, 0.0015 →0.0004 cm^3/g) when steam was used as the gasification medium. Additionally, SEM analysis further revealed that smaller NS1100 particles tended to merge into larger agglomerates during the gasification process, resulting in clustered structures in the reacted OC samples. This behavior can be attributed to the accelerated agglomeration tendency of alkali compounds (e.g., K and Na) under steam-rich conditions [55]. Additionally, steam promotes the formation of alkali silicates and alkali hydroxides, which lowers their melting points and increases particle wettability, further enhancing agglomeration. This partial deactivation of the OC is further supported by the narrowing differences in product gas composition, syngas yields, CCE and CGE values between CBGAS and BCLGS at higher temperatures, as illustrated in Fig. 9(b).

Furthermore, analysis of the CCE trend revealed that at reactor temperatures of 850 and 900 °C, CCE was higher in BCLGS compared to CBGAS (≈ +1.4%). It can be attributed to the improved conversion of residual carbon facilitated by the promotion of the water–gas reaction

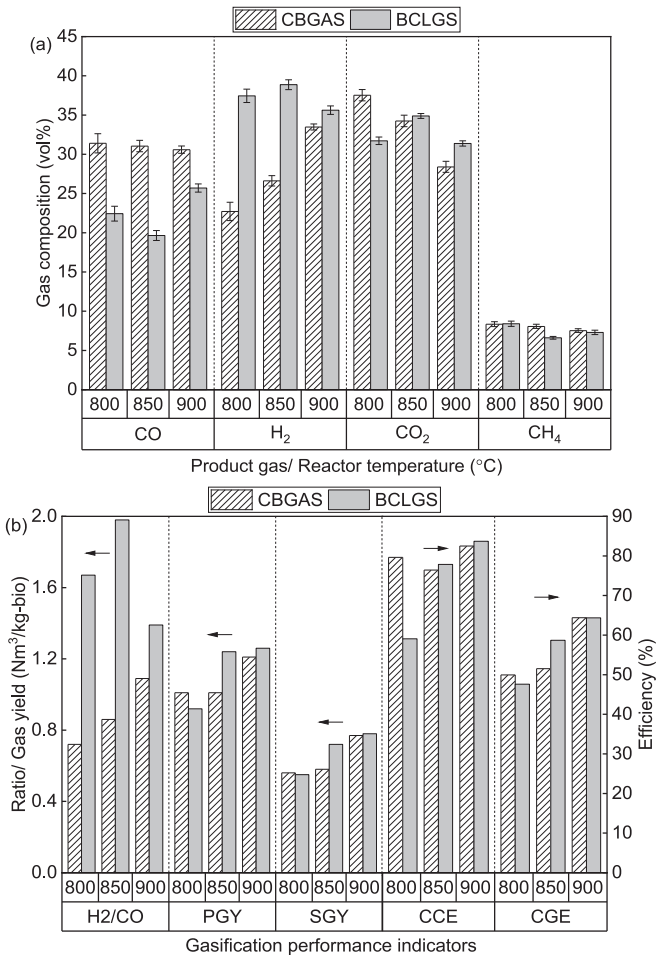

Fig. 9. Comparison of (a) product gas composition and (b) H_2/CO ratio, PGY, SGY, carbon conversion and cold gasification efficiency between conventional biomass gasification using air/steam and biomass chemical looping gasification with steam. Here, PGY and SGY denotes product gas yield and syngas yields, respectively.

(R3). Moreover, at 800 °C, BCLGS exhibited inferior gasification performance compared to CBGAS with lower gas yields (≈ −0.05 Nm^3/kg-bio) and efficiencies (CCE ≈ −20.5% and CGE ≈ −2.5%). It may be ascribed to insufficient activation of the OC at lower temperatures. Ultimately, it can be considered that a reactor temperature of 850 °C was ideal, where the OC is optimally activated to promote gasification reactions and achieve enhanced performance.

3.3.3. *Comprehensive evaluation*

Reflecting on the objective of the study to benchmark chemical looping against conventional gasification methods, the gasification methods CBGA, CBGAS, BCLGO and BCLGS were thoroughly investigated to provide a deeper understanding of the potential benefits and limitations. These methods underwent thorough analysis covering crucial gasification performance indicators, including product gas composition, syngas and product gas yields, carbon conversion and cold gas efficiencies. To this end, the integration of results from these investigations is pivotal in facilitating a comprehensive evaluation of the most suitable gasification method. The comparison results among different gasification methods, depicted in Fig. 10, provide valuable insights for drawing conclusions. The results are comparative considering all the experiments were carried out under similar conditions with a reactor temperature of 850 °C and a PFR feed rate of 1.1 g/min. For CBGA and CBGAS configurations, the airflow rate was held constant at 0.09 Nm^3/h, which correspond to an ER of 0.27. In contrast, for the

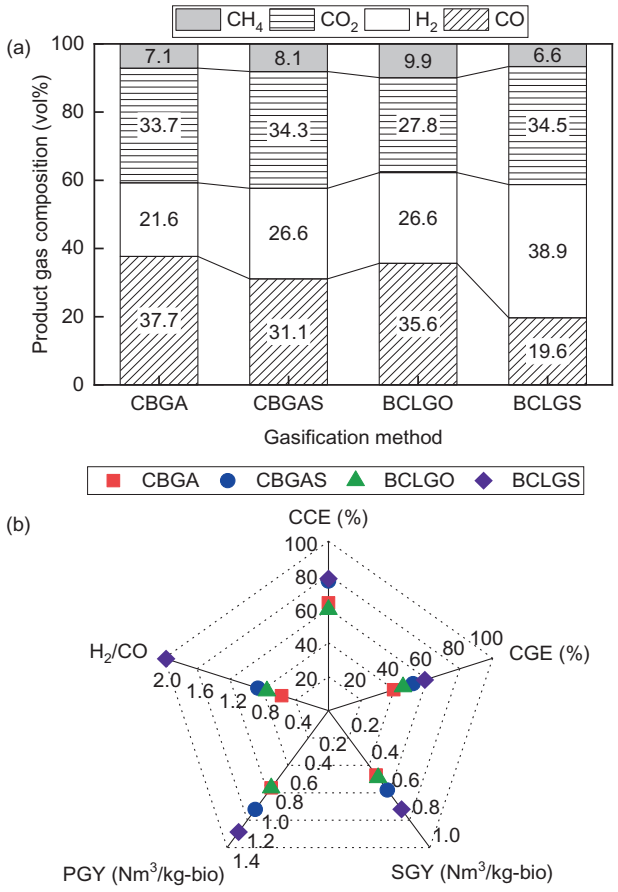

Fig. 10. Overall comparison of (a) product gas composition and (b) carbon conversion and cold gasification efficiency, SGY, PGY and H_2/CO ratio among different gasification methods. Here, SGY and PGY denotes syngas yield and product gas yields, respectively.

BCLG configuration, oxygen source was changed from air to OC, with an OCBR of 10:1 and yielded a similar ER of 0.25. Additionally, the SBR was controlled within the range of 1.3 to 1.4 for CBGAS and BCLGS configurations.

The analysis of Fig. 10 reveals that gasification methods, including CBGA, CBGAS and BCLGO, exhibit similar compositions within specific ranges: CO concentration ranged between 36.6–37.7 vol%, H_2 concentration ranged from 21.6-26.6 vol%, CO_2 concentration ranged between 27.8–34.3 vol%, and CH_4 concentration lied within 7.1–9.9 vol%. However, a notable deviation in composition is observed for BCLGS, characterized by a substantial increase in H_2 concentration to 38.9 vol%, accompanied by a decrease in CO concentration to 19.6 vol%, and CH_4 concentration to 6.6%, while CO_2 concentration remained relatively similar at 34.5 vol%. The change in composition can be predominantly attributed to enhanced reforming reactions (water–gas reaction, R3, water–gas shift reaction, R4, and steam-methane reforming reaction, R5), facilitated by two key factors; the addition of steam as a gasification medium and more importantly the catalytic properties of OC material. Consequently, the elevated H_2 concentration rendered BCLGS particularly suitable for H_2 production. Additionally, BCLGS demonstrated superior gasification performance demonstrated by its highest CCE at 77.9%, CGE at 58.7%, H_2/CO ratio of 1.99, and the best syngas and product gas yields of 0.7 and 1.2 Nm^3/kg-bio, respectively. Interestingly, the H_2/CO ratio of 2.0 observed in BCLGS aligns well with the requirements for biofuel production (e.g. Fischer–Tropsch liquids, SNG, ammonia or methanol), potentially eliminating the need for additional reactors to adjust this ratio. While conventional gasification methods typically exhibit H_2/CO ratios below 1, BCLGS presents a promising solution to overcome this limitation. Nevertheless, CBGA, CBGAS and BCLGO remain viable options for gasoline production, which requires a H_2/CO ratio of 0.5 to 1.0. In the context of BCLGO, it demonstrated similar performance to that of CBGA, albeit with inferior performance relative to CBGAS. It is characterized by inferior CCE (59.69%) than that of CBGA and CBGAS. Moreover, its CGE of 45.43% was slightly higher compared to CBGA but lower than CBGAS. Additionally, the BCLGO yielded a product gas yield of 0.79 Nm^3/kg-bio, which was equivalent to CBGA but lower than CBGAS. Similarly, its syngas yield of 0.49 Nm^3/kg-bio marginally exceeded CBGA but trailed behind CBGAS. Notably, the H_2/CO ratio of BCLGO measured at 0.75 exceeded that of CBGA but was less than that of CBGAS. In conclusion, while BCLGO demonstrated comparable performance to conventional gasification methods, BCLGS emerged as a promising alternative to conventional gasification. BCLGS outperformed all other methods across the measured gasification performance indicators.

The study demonstrated that BCLGS is a promising alternative to conventional gasification methods. However, agglomeration due to sintering, particularly at high temperatures in the presence of steam, remains a challenge, as discussed in detail in our previous study [43]. Additionally, experiments were carried out using a lab-scale (~0.5 kW_{th}) bubbling fluidized bed reactor with fresh OC material for each test, subjecting the particles to less stress than would occur in a circulating fluidized bed system. Moreover, it was assumed that the lattice oxygen supplied by NS1100 is constant, based on the material's oxygen transport capacity, without accounting for the kinetic effects of particle size or reaction time. Consequently, further research is needed to investigate and optimize particle size, residence time, and incorporate advanced reactor designs (e.g., dual fluidized beds) to improve performance and scalability. To this end, pilot-scale testing is also essential to evaluate long-term durability and attrition behavior of OC material. For a detailed discussion of the challenges associated with nickel smelter slag and perspective on its advancement for BCLG applications, refer to our previous study on evaluation of nickel smelter slag for BCLG [43].

4. Conclusion

This study primarily compared the performance of biomass chemical looping gasification (BCLG) against conventional gasification methods such as air and air/steam. It analyzed the impact of different operational parameters on the conventional gasification of pine forest residue and concluded that a reactor temperature of 900 °C, an equivalence ratio of 0.3 and the steam-to-biomass ratio of 1.3 were the most optimal parameters. The comparison of different gasification methods suggested that BCLG without steam exhibited performance similar to conventional biomass gasification using air and air/steam, which can be attributed to the limited interaction efficiency of oxygen carrier particles with biomass volatiles. Additionally, BCLG with steam outperformed all other methods and emerged as the most promising alternative to conventional gasification. BCLGS demonstrated improvements of approximately 111% in the H_2/CO ratio, 30% in product gas yield, 17% in syngas yield, 2% in carbon conversion efficiency and 14% in cold gasification efficiency, compared to conventional biomass gasification using air/steam. It can be concluded that the presence of oxygen carrier catalyzed the reforming reactions, thereby significantly enhancing the performance of BCLG with steam.

CRediT authorship contribution statement

Avishek Goel: Writing – original draft, Visualization, Methodology, Investigation, Funding acquisition, Formal analysis, Conceptualization. **Fabiola Panitz:** Writing – review & editing, Resources. **Elyas M. Moghaddam:** Writing – review & editing. **Jochen Ströhle:** Writing – review & editing, Resources. **Bernd Epple:** Writing – review & editing, Resources. **Chao He:** Writing – review & editing, Supervision. **Jukka**

Konttinen: Writing – review & editing, Supervision, Methodology, Funding acquisition.

Declaration of competing interest

The authors declare that they have no known competing financial interests or personal relationships that could have appeared to influence the work reported in this paper.

Acknowledgements

This work is supported by Tampere University and Climate Neutral Energy Systems and Society (CNESS) and the Technical University of Darmstadt, Germany. The authors would like to acknowledge the support of Leo Hyvärinen, Kati Valtonen, Merja Ritola and Turkka Salminen during the characterization of materials. The authors would also like to acknowledge Boliden for providing nickel smelter slag utilized in the study. C. H. acknowledges the Academy Research Fellowship and its related research project funded by Research Council of Finland (decision numbers: 341052, 346578).

Appendix A. Supplementary data

Supplementary data to this article can be found online at https://doi.org/10.1016/j.ecmx.2026.101828.

Data availability

Data will be made available on request.

References

[1] S. Oksanen, Advanced biofuels: What holds them back?, International Renewable Energy Agency, Abu Dhabi, 2019. www.irena.org/publications.
[2] Ge H, Guo W, Shen L, Song T, Xiao J. Experimental investigation on biomass gasification using chemical looping in a batch reactor and a continuous dual reactor. Chem Eng J 2016;286:689–700. https://doi.org/10.1016/j.cej.2015.11.008.
[3] Song F, Tan Y, Xie H, Zhang Q, Han Y. Direct synthesis of dimethyl ether from biomass-derived syngas over Cu–ZnO–Al2O3–ZrO2(x)/γ-Al2O3 bifunctional catalysts: effect of Zr-loading. Fuel Process Technol 2014;126:88–94. https://doi.org/10.1016/j.fuproc.2014.04.021.
[4] Woolcock PJ, Brown RC. A review of cleaning technologies for biomass-derived syngas. Biomass Bioenergy 2013;52:54–84. https://doi.org/10.1016/j.biombioe.2013.02.036.
[5] Goel A, Moghaddam EM, Liu W, He C, Konttinen J. Biomass chemical looping gasification for high-quality syngas: a critical review and technological outlooks. Energ Conver Manage 2022;268:116020. https://doi.org/10.1016/j.enconman.2022.116020.
[6] S. De, A.K. Agarwal, V. Moholkar, B. Thallada, Coal and biomass gasification, Energy, Environment, and Sustainability (2018).
[7] Huang Z, Zhang Y, Fu J, Yu L, Chen M, Liu S, et al. Chemical looping gasification of biomass char using iron ore as an oxygen carrier. Int J Hydrogen Energy 2016;41:17871–83.
[8] Ge H, Zhang H, Guo W, Song T, Shen L. System simulation and experimental verification: biomass-based integrated gasification combined cycle (BIGCC) coupling with chemical looping gasification (CLG) for power generation. Fuel 2019;241:118–28. https://doi.org/10.1016/j.fuel.2018.11.091.
[9] L.-S. Fan, E.Y. Chung, S.C. Bayham, M.V. Kathe, A. Tong, L. Zeng, Chemical looping combustion and gasification, in: Handbook of Clean Energy Systems, John Wiley & Sons, Ltd, 2015: pp. 1–22. https://doi.org/10.1002/9781118991978.hces150.
[10] Wei G, He F, Huang Z, Zheng A, Zhao K, Li H. Continuous operation of a 10 kW $_{th}$ chemical looping integrated fluidized bed reactor for gasifying biomass using an iron-based oxygen carrier. Energy Fuels 2015;29:233–41. https://doi.org/10.1021/ef5021457.
[11] Moldenhauer P, Linderholm C, Rydén M, Lyngfelt A. Avoiding CO2 capture effort and cost for negative CO2 emissions using industrial waste in chemical-looping combustion/gasification of biomass. Mitig Adapt Strateg Glob Change 2020;25:1–24. https://doi.org/10.1007/s11027-019-9843-2.
[12] Lin Y, Wang H, Wang Y, Huo R, Huang Z, Liu M, et al. Review of biomass chemical looping gasification in China. Energy Fuel 2020;34:7847–62.
[13] Mendiara T, García-Labiano F, Abad A, Gayán P, De Diego L, Izquierdo M, et al. Negative CO2 emissions through the use of biofuels in chemical looping technology: a review. Appl Energy 2018;232:657–84.
[14] Mendiara T, Johansen JM, Utrilla R, Geraldo P, Jensen AD, Glarborg P. Evaluation of different oxygen carriers for biomass tar reforming (I): carbon deposition in experiments with toluene. Fuel 2011;90:1049–60. https://doi.org/10.1016/j.fuel.2010.11.028.
[15] Sonoyama N, Nobuta K, Kimura T, Hosokai S, Hayashi J, Tago T, et al. Production of chemicals by cracking pyrolytic tar from Loy Yang coal over iron oxide catalysts in a steam atmosphere. Fuel Process Technol 2011;92:771–5. https://doi.org/10.1016/j.fuproc.2010.09.036.
[16] Cao J-P, Shi P, Zhao X-Y, Wei X-Y, Takarada T. Catalytic reforming of volatiles and nitrogen compounds from sewage sludge pyrolysis to clean hydrogen and synthetic gas over a nickel catalyst. Fuel Process Technol 2014;123:34–40. https://doi.org/10.1016/j.fuproc.2014.01.042.
[17] Acharya B, Dutta A, Basu P. Chemical-looping gasification of biomass for hydrogen-enriched gas production with in-process carbon dioxide capture. Energy Fuels 2009;23:5077–83. https://doi.org/10.1021/ef9003889.
[18] Wei G, He F, Huang Z, Zheng A, Zhao K, Li H. Continuous operation of a 10 kWth chemical looping integrated fluidized bed reactor for gasifying biomass using an iron-based oxygen carrier. Energy Fuels 2015;29:233–41. https://doi.org/10.1021/ef5021457.
[19] O. Condori, F. García-Labiano, F. Luis, M.T. Izquierdo, A. Abad, J. Adánez, Biomass chemical looping gasification for syngas production using LD Slag as oxygen carrier in a 1.5 kWth unit, Fuel Processing Technology 222 (2021) 106963. https://doi.org/https://doi.org/10.1016/j.fuproc.2021.106963.
[20] Hu J, Li C, Lee D-J, Guo Q, Zhao S, Zhang Q, et al. Syngas production from biomass using Fe-based oxygen carrier: optimization. Bioresour Technol 2019;280:183–7. https://doi.org/10.1016/j.biortech.2019.02.012.
[21] Wei G, He F, Zhao Z, Huang Z, Zheng A, Zhao K, et al. Performance of Fe–Ni bimetallic oxygen carriers for chemical looping gasification of biomass in a 10 kWth interconnected circulating fluidized bed reactor. Int J Hydrogen Energy 2015;40:16021–32. https://doi.org/10.1016/j.ijhydene.2015.09.128.
[22] Shen X, Yan F, Zhang Z, Li C, Zhao S, Zhang Z. Enhanced and environment-friendly chemical looping gasification of crop straw using red mud as a sinter-resistant oxygen carrier. Waste Manag 2021;121:354–64.
[23] Ge H, Guo W, Shen L, Song T, Xiao J. Biomass gasification using chemical looping in a 25 kWth reactor with natural hematite as oxygen carrier. Chem Eng J 2016;286:174–83. https://doi.org/10.1016/j.cej.2015.10.092.
[24] Condori O, de Diego LF, Garcia-Labiano F, Izquierdo MT, Abad A, Adánez J. Syngas production in a 1.5 kWth biomass chemical looping gasification unit using Fe and Mn ores as the oxygen carrier. Energy Fuel 2021;35:17182–96. https://doi.org/10.1021/acs.energyfuels.1c01878.
[25] Huseyin S, Wei G, Li H, He F, Huang Z. Chemical-looping gasification of biomass in a 10 kWth interconnected fluidized bed reactor using Fe2O3/Al2O3 oxygen carrier. J Fuel Chem Technol 2014;42:922–31. https://doi.org/10.1016/S1872-5813(14)60039-6.
[26] Huang Z, He F, Feng Y, Zhao K, Zheng A, Chang S, et al. Biomass char direct chemical looping gasification using NiO-modified iron ore as an oxygen carrier. Energy Fuel 2014;28:183–91.
[27] Dieringer P, Marx F, Lebendig F, Müller M, Di Giuliano A, Gallucci K, et al. Fate of ilmenite as oxygen carrier during 1 MWth chemical looping gasification of biogenic residues. Appl Energy Combust Sci 2023;16:100227. https://doi.org/10.1016/j.jaecs.2023.100227.
[28] Marx F, Dieringer P, Ströhle J, Epple B. Process efficiency and syngas quality from autothermal operation of a 1 MWth chemical looping gasifier with biogenic residues. Appl Energy Combust Sci 2023;16:100217. https://doi.org/10.1016/j.jaecs.2023.100217.
[29] Li Z, Li J, Wang Y, Li W, Wei G, Liu X, et al. Demonstration of biomass chemical looping gasification in a 5 MWth pilot unit using ilmenite as oxygen carrier. Fuel 2026;405:136472. https://doi.org/10.1016/j.fuel.2025.136472.
[30] P. Dieringer, Demonstration and Optimization of the Chemical Looping Gasification Technology in 1 MWth Scale, (2024). https://doi.org/10.26083/tuprints-00026623.
[31] Hu J, Li C, Guo Q, Dang J, Zhang Q, Lee D-J, et al. Syngas production by chemical-looping gasification of wheat straw with Fe-based oxygen carrier. Bioresour Technol 2018;263:273–9. https://doi.org/10.1016/j.biortech.2018.02.064.
[32] Huang Z, He F, Zhu H, Chen D, Zhao K, Wei G, et al. Thermodynamic analysis and thermogravimetric investigation on chemical looping gasification of biomass char under different atmospheres with Fe2O3 oxygen carrier. Appl Energy 2015;157:546–53.
[33] Hatano H. Low temperature gasification using lattice oxygen. Chem Eng Sci 2010;65:47–53. https://doi.org/10.1016/j.ces.2009.01.061.
[34] Huang Z, Xu G, Deng Z, Zhao K, He F, Chen D, et al. Investigation on gasification performance of sewage sludge using chemical looping gasification with iron ore oxygen carrier. Int J Hydrogen Energy 2017;42:25474–91. https://doi.org/10.1016/j.ijhydene.2017.08.133.
[35] Hu J, Li C, Zhang Q, Guo Q, Zhao S, Wang W, et al. Using chemical looping gasification with Fe2O3/Al2O3 oxygen carrier to produce syngas (H2+ CO) from rice straw. Int J Hydrogen Energy 2019;44:3382–6. https://doi.org/10.1016/j.ijhydene.2018.06.147.
[36] Hu Q, Shen Y, Chew JW, Ge T, Wang C-H. Chemical looping gasification of biomass with Fe2O3/CaO as the oxygen carrier for hydrogen-enriched syngas production. Chem Eng J 2020;379:122346.
[37] Shen T, Ge H, Shen L. Characterization of combined Fe-Cu oxides as oxygen carrier in chemical looping gasification of biomass. Int J Greenhouse Gas Control 2018;75:63–73.
[38] Yang H, Liao Y, Huang J, Chen Y, Ma X. Chemical looping gasification of pine wood over layer-confined Ni: loading-packing synergy and cyclic stability. Energy 2026;347:140283. https://doi.org/10.1016/j.energy.2026.140283.

[39] Jiang Y, Ge H, Wang P, Zhang T, Tan R, Song T. Syngas upgrading and tar mitigation from microalgal residues: pelletization–torrefaction pretreatment and chemical looping gasification. J Anal Appl Pyrol 2026;195:107666. https://doi.org/10.1016/j.jaap.2026.107666.
[40] An F, Xi S, Wang S, Gai D, Wang X, Zhong Z, et al. Chemical looping gasification of water-containing biomass using red mud as an oxygen carrier. Energy Fuels 2026;40:2812–25. https://doi.org/10.1021/acs.energyfuels.5c05626.
[41] Fang S, Ding L, Lin Y, Yan S, Zheng X, Huang Z, et al. Analysis of nitrogen distribution in chemical looping gasification of kitchen waste and soy protein as a model compound with CuFe2O4 and NiFe2O4 oxygen carriers. Fuel 2026;414:138292. https://doi.org/10.1016/j.fuel.2026.138292.
[42] Domingos Y, de Las Obras M, Loscertales MT, Izquierdo AA. Syngas production from liquid and solid fractions of swine manure in a 0.5 kWth chemical looping gasification unit. Energies 2026;19:317. https://doi.org/10.3390/en19020317.
[43] Goel A, Panitz F, Moghaddam EM, Ströhle J, Epple B, He C, et al. Performance evaluation of biomass chemical looping gasification in a fluidized bed reactor using industrial waste as oxygen carrier. Bioresour Technol 2025;427:132447. https://doi.org/10.1016/j.biortech.2025.132447.
[44] Goel A, Ismailov A, Moghaddam EM, He C, Konttinen J. Evaluation of low-cost oxygen carriers for biomass chemical looping gasification. Chem Eng J 2023;469:143948. https://doi.org/10.1016/j.cej.2023.143948.
[45] Wei L, Zhu F, Li Q, Xue C, Xia X, Yu H, et al. Development, current state and future trends of sludge management in China: based on exploratory data and CO2-equivaient emissions analysis. Environ Int 2020;144:106093.
[46] Liu L, Huang Y, Cao J, Liu C, Dong L, Xu L, et al. Experimental study of biomass gasification with oxygen-enriched air in fluidized bed gasifier. Sci Total Environ 2018;626:423–33. https://doi.org/10.1016/j.scitotenv.2018.01.016.
[47] Niu M, Huang Y, Jin B, Sun Y, Wang X. Enriched-air gasification of refuse-derived fuel in a fluidized bed: effect of gasifying conditions and bed materials. Chem Eng Technol 2014;37:1787–96. https://doi.org/10.1002/ceat.201400167.
[48] Han SW, Lee JJ, Tokmurzin D, Lee SH, Nam JY, Park SJ, et al. Gasification characteristics of waste plastics (SRF) in a bubbling fluidized bed: effects of temperature and equivalence ratio. Energy 2022;238:121944. https://doi.org/10.1016/j.energy.2021.121944.
[49] Gomes HGMF, Matos MAA, Tarelho LAC. Influence of oxygen/steam addition on the quality of producer gas during direct (air) gasification of residual forest biomass. Energies 2023;16:2427. https://doi.org/10.3390/en16052427.
[50] Hernández JJ, Aranda G, Barba J, Mendoza JM. Effect of steam content in the air–steam flow on biomass entrained flow gasification. Fuel Process Technol 2012;99:43–55. https://doi.org/10.1016/j.fuproc.2012.01.030.
[51] Nguyen NM, Alobaid F, May J, Peters J, Epple B. Experimental study on steam gasification of torrefied woodchips in a bubbling fluidized bed reactor. Energy 2020;202:117744. https://doi.org/10.1016/j.energy.2020.117744.
[52] Deng ZG, Xiao R, Jin BS, Song QL, Huang H. Multiphase CFD modeling for a chemical looping combustion process (fuel reactor). Chem Eng Technol 2008;31:1754–66. https://doi.org/10.1002/ceat.200800341.
[53] M.M. Sheth, A.B. Harichandan, Effect of oxygen carrier particle size on the hydrodynamics of fuel reactor in a chemical looping combustion system, 06 (2017). www.ijarse.com.
[54] Hu Z, Jiang E, Ma X. The effect of oxygen carrier content and temperature on chemical looping gasification of microalgae for syngas production. J Energy Inst 2019;92:474–87. https://doi.org/10.1016/j.joei.2018.05.001.
[55] L. Zhao, Agglomeration during Fluidized Bed Combustion and Gasification of Biomass, (2021).